Excitability in a stochastic differential equation model for calcium puffs

S. Rüdiger
Institut für Physik, Humboldt-Universität zu Berlin, 12489 Berlin, Germany
(Received 19 October 2013; revised manuscript received 19 February 2014; published 27 June 2014)

Calcium dynamics are essential to a multitude of cellular processes. For many cell types, localized discharges of calcium through small clusters of intracellular channels are building blocks for all spatially extended calcium signals. Because of the large noise amplitude, the validity of noise-approximating model equations for this system has been questioned. Here we revisit the master equations for local calcium release, examine the multiple scales of calcium concentrations in the cluster domain, and derive adapted stochastic differential equations. We show by comparison of discrete and continuous trajectories that the Langevin equations can be made consistent with the master equations even for very small channel numbers. In its deterministic limit, the model reveals that excitability, a dynamical phenomenon observed in many natural systems, is at the core of calcium puffs. The model also predicts a bifurcation from transient to sustained release which may link local and global calcium signals in cells.

DOI: 10.1103/PhysRevE.89.062717 PACS number(s): 87.16.Xa, 05.10.Gg, 05.45.−a, 87.10.Mn

I. INTRODUCTION

Repetitive increases in intracellular Ca^{2+} concentrations control various physiological functions, including muscle cell contraction, neurotransmitter secretion, and gene expression [1]. In many cells, Ca^{2+} levels rise after stimulation by extracellular signals. If the stimulation is small, Ca^{2+} is released in a spatially confined way from clusters of intracellular Ca^{2+} channels. Here, molecular interactions within a single cluster lead to coherent opening of its channels and result in elementary events called sparks or puffs [2,3]. For larger stimulation, Ca^{2+} forms spatiotemporal waves or whole-cell oscillations involving release by many clusters. The transition from local puffs to global waves and oscillations is a prime example to study the onset of collective activity in cells.

In recent years various physical concepts of emergent phenomena have been invoked to link local and global dynamics, among them percolation [4], nucleation [5], and self-organized criticality [6]. However, no model has been proposed that correctly represents dynamics at all levels of complexity, from single channel gating to puffs and whole-cell release. A chief obstacle for a consensual theory is the high level of noise, which is caused by the low number of ion channels per cluster. Consequently, recent models of Ca^{2+} puffs observed in electrically nonexcitable cells have been mathematically expressed with discrete stochastic variables and master equations [7]. A number of studies have indicated that these models can generally reproduce the experimental observations [8–10], but a deeper understanding of the underlying dynamics remained elusive.

To tackle this problem we here derive continuous rate equations for local signals. Our approach invokes the standard Kramers-Moyal expansion of the governing master equations, but it incorporates in a nonstandard way the dependence of local Ca^{2+} concentration on the number of open channels. We carry over the discreteness of the Markov chain close to the rest state while approximating it with the continuum description for the fast evolution during a puff [11]. This method resolves the limitation of prior attempts at Langevin modeling of Ca^{2+} puffs, which were consistent for large numbers of channels only [12,13]. In fact, the number of channels N in a cluster is small ($N \approx 10$), and an earlier study had concluded that noise would be too large to use approximations with continuous channel fractions [14]. In contrast, here we demonstrate that consistent Langevin equations can be derived when they are adapted to the intracluster distribution of Ca^{2+} and when "microscopic" parameters are chosen in accord with single channel behavior.

Simulations with the resulting set of stochastic differential equations are compared to those with the original discrete model and with recent experimental findings showing the validity of our approach. Langevin equations for Ca^{2+} puffs are thus useful and accurate even for realistically low channel numbers. Importantly our mathematical model allows the analysis of its deterministic limit using methods from dynamical systems theory. The nonlinear analysis reveals the excitability at the core of the equations. Since excitable systems necessitate perturbations or noise for nontrivial dynamics, our analysis thus provides clear evidence for the noise-induced nature of Ca^{2+} puffs.

Finally, when we increase the number of channels in a cluster, we find a bifurcation from excitable to bistable behavior. The bistability causes a biphasic release dynamics very much resembling that of global Ca^{2+} release seen in oocytes [15]. This suggests that the puff-to-wave transition is a bifurcation in the *local* dynamical behavior and that the bifurcation mediates global synchronization. Our results thus shed light on the poorly understood functioning of local Ca^{2+} signaling and may lead to a novel understanding of whole-cell signals.

II. DERIVATION OF A MINIMAL DISCRETE MODEL

We start with the channel scheme of De Young and Keizer (DYK) [16], which models the relevant molecular processes of a single inositol 1,4,5-trisphosphate receptor (IP_3R) channel [17]. IP_3Rs are Ca^{2+} release channels located in the membrane of the endoplasmic reticulum (ER). They open in response to increased cytosolic concentrations of IP_3 produced *in vivo* after hormone stimulation of cells. The basic molecular interactions of the channel include the binding of IP_3 and Ca^{2+} to the receptor promoting the opening of a channel as well as

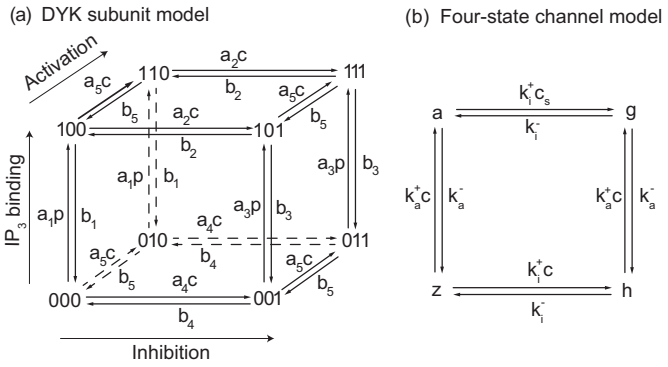

FIG. 1. (a) Markov chain model of the gating behavior of a single subunit of the IP_3R channel according to the DYK model. Channel states (000, 100, . . .) are denoted with respect to the binding state (unbound 0, bound 1) of the IP_3 binding site, the activating Ca^{2+} binding site, and the inhibiting Ca^{2+} binding site, respectively. c denotes Ca^{2+} concentration and p denotes IP_3 concentration. (b) Four-state Markov chain of the channel-based model derived in this study. The state a represents the open channel. An upward transition corresponds to activation, whereas a transition to the right corresponds to inhibition.

inhibitory binding of Ca^{2+} closing the channel. IP_3 receptors are tetramers, and we will initially assume that each of the three types of binding sites occurs on each of the four IP_3R subunits, see Fig. 1(a). Because of experimental evidence of subunit cooperativity we assume that a channel is open if at least three of its four subunits have IP_3 and activating Ca^{2+} bound but inhibiting Ca^{2+}unbound [state 110 in Fig. 1(a)]. Released Ca^{2+} of an open channel spreads within the surroundings and triggers other channels to open.

In our previous papers [8,18,19] we have considered a detailed three-dimensional reaction-diffusion model for spreading Ca^{2+}. The main conclusion of this analysis was that Ca^{2+} released from spatially separated channels remains inhomogeneously distributed within the cluster domain. Because of the large difference in Ca^{2+} concentration in the ER store and cytosol, steep gradients around each open channel occur, which roughly correspond to the $1/r$ solution of the three-dimensional Laplace equation for point sources. As a result, Ca^{2+} profiles of open channels partly overlap, but the extent and the significance of this overlap depend on the distance of channels in the cluster. Since the distance of channels is not directly known from experiments, in Ref. [8] we set out to estimate it. We compared detailed numerical simulations with experimental puff data using the channel distance as a free parameter in our model. We found that the broad distribution of puff peak amplitudes in mammalian cells [20] is matched best in a model of large channel distance and small domain overlap so that $[Ca^{2+}]$ at adjacent channels is an order of magnitude smaller than the Ca^{2+} at the open channel. Intuitively, this can be understood from the fact that coupling of channels in a tight cluster would inhibit some channels in an active cluster before they open and thus yield a decaying amplitude distribution very different from the experimentally observed broad distribution [8].

Hence, the action of released Ca^{2+} on the receptors has to be distinguished according to its $[Ca^{2+}]$ scale. At an open channel, Ca^{2+} concentration is high, and binding to the receptor is relatively fast (feedback Ca^{2+} scale). Further away from the open channel—at locations of closed channels in the cluster—Ca^{2+} concentration measures on a much smaller scale. This Ca^{2+} is particularly important for propagation of channel activation within the cluster (Ca^{2+} feedforward). Therefore, in our model we will distinguish the feedback at high Ca^{2+} concentration, denoted c_s below, onto a releasing channel from the feedforward, at lower Ca^{2+} concentration c, directed at closed channels in the cluster [8,21].

The finding that Ca^{2+} coupling in the cluster separates into the two scales implies that mean concentrations of Ca^{2+} and fractions of bound ligand sites cannot be introduced in a straightforward way. Said in another way, the assumption of mixing between receptor channels and their ligands does not hold, and it is thus difficult to derive models based on populations of binding sites as was performed by Hodgkin and Huxley for neuronal action potentials [22]. Since binding sites of IP_3R channels in the cluster may experience different Ca^{2+} concentrations, one needs to distinguish them depending on whether they belong to an open or a closed channel. For instance, an inhibitory subunit which belongs to an open channel is subjected to much higher $[Ca^{2+}]$ than a subunit that belongs to a closed channel. This introduces a correlation in the binding probability. In simulations, for each channel the state of all subunits must be stored, and a reduction to simple activating and inhibiting gating variables is not possible. Rather, the channel's state must be assigned to a node on a large transition space. Since each subunit allows for 8 different states in the DYK model, the complete transition lattice consists of 8^4 states, which is far too large to be used for a differential equation model.

Our aim is therefore to drastically reduce the number of channel states in the tetrameric DYK model by eliminating the subunit dynamics and derive a small Markov chain for the state of the entire channel. First, we ignore the IP_3 binding and unbinding by invoking the relatively high IP_3 concentration under which Ca^{2+} puff experiments are performed. The IP_3 binding sites can then simply be assumed to be saturated. Alternatively, lower IP_3 concentration can be converted into a smaller total number of channels N. Then, in the subunit-free gating scheme considered in the following, each channel can assume one of four remaining states of the upper plane in the DYK box: a rest state (denoted z instead of 100 to distinguish the channel state z from the subunit state 100), an open state with activating Ca^{2+} bound (a), a closed state with both activating and inhibiting Ca^{2+} bound (g), and a closed state with inhibiting Ca^{2+} bound (h), see Fig. 1(b). Transition rates are calculated from the rates $k^{\pm}_{a,i}$ and the c and c_s values if applicable. Note that for an open channel residing in state a, the only transition involving Ca^{2+} binding is determined by the large-scale Ca^{2+} concentration c_s, whereas for a closed channel (states z and h) Ca^{2+} binding occurs based on c.

In the scheme in Fig. 1(b), the individual transition rates are to be determined from the effective rates between the compound states based on the original subunit dynamics.

Transitions on lattices of subunit states may result in nontrivial kinetic rates of transitions between compound states. However, preliminary simulations have shown that here the subunit dynamics is significant mostly for the rate of generation of puffs and not as much for their termination. Therefore, all reactions in the four-state model are here chosen to be of standard zero or first order except for the transition from z to a.

To calculate the rate of the z-a transition of a single channel, we have to consider the mean first passage time for a transition from the rest to the open state in the tetrameric DYK model. The refractory period due to inhibition is typically short so that it can be assumed that all four subunits may be involved in the activation process. In the tetrameric DYK model, the open transition occurs as a transition between a state with two activated subunits to the one with three activated subunits, and we thus need to calculate the mean first passage time of this transition. This can simply be performed in the following way: The probability that a single subunit is activated is $P_{\rm act} = a_5 c/(a_5 c + b_5)$. Here a_5 and b_5 denote the forward and backward rates of the activating Ca^{2+} binding [see Fig. 1(a)]. The probabilities that none, one, or two of the four subunits are activated thus are as follows: $P_0 = (1 - P_{\rm act})^4$, $P_1 = 4P_{\rm act}(1 - P_{\rm act})^3$, and $P_2 = 6P_{\rm act}^2(1 - P_{\rm act})^2$. The probability to be in state P_2 provided that the channel is not open, is

$$P(2|\{0,1,2\}) = \frac{P_2}{P_0 + P_1 + P_2}. \tag{1}$$

The rate of escaping the z state can be calculated as $k_a^+ c$ with

$$k_a^+(c) = 2a_5 P(2|\{0,1,2\}).$$

Thus, in our four-state scheme $k_{\rm a}^+ = k_{\rm a}^+(c)$ depends in a strongly nonlinear way on the mean cluster concentration c (see below), whereas all other $k_{\rm a,i}^{+,-}$'s are constant parameters. The activation rate $k_{\rm a}^+$ can be estimated from the activation and deactivation constants a_5 and b_5 given below.

The mean cluster concentration was defined in dependence on the number of open channels n (i.e., the number of channels in state a), based on spatial numerical simulations [8],

$$c_{\rm d}(n) = c_0 + c_1 n, \tag{2}$$

where c_0 is the rest level concentration (here taken at 0.025 μM) and c_1 is a coupling constant ($c_1 = 0.74$ μM). We have here introduced the variable $c_{\rm d}(n)$, which gives the typical intracluster Ca^{2+} concentration for a quasistationary number of open channels. In a time-dependent setting, i.e., after opening or closing of a channel, we postulate, most simply, that the c variable obeys equilibration with rate λ,

$$\frac{dc}{dt} = \lambda(c_{\rm d} - c). \tag{3}$$

In the following, however, we study the case of large λ ($\lambda = 1000$ s^{-1}) in accordance with our earlier finding that small λ is incompatible with the presence of Ca^{2+} puffs [18] and the lacking evidence of slow domain collapse in puff experiments [20].

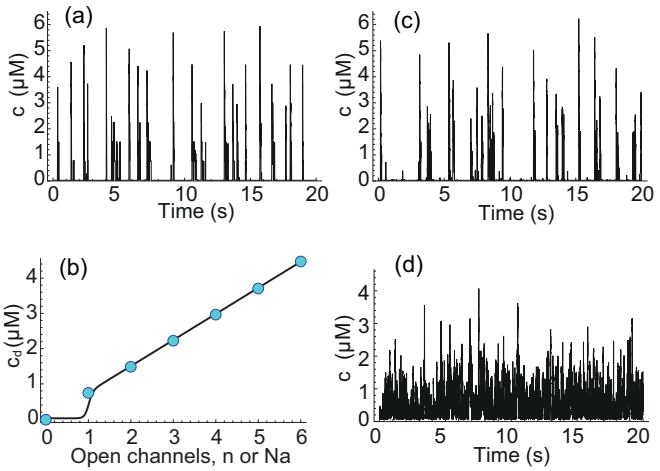

FIG. 2. (Color online) (a) Evolution of Ca^{2+} concentration $c(t)$ in simulations with $N = 10$ channels in the discrete model four-state model. (b) Graph of domain Ca^{2+} concentration in dependence on open-channel numbers for the discrete model (dots) and the continuous model [line: Eq. (4), with $N = 6$, $c_0 = 0.025$ μM, and $c_1 = 0.74$ μM]. (c) Evolution of $c(t)$ in simulations with $N = 10$ channels for the Langevin model. (d) Illustration of the failure of puff generation in a standard continuous representation using $c_{\rm d}(a) = c_0 + c_1 Na$ instead of Eq. (4).

III. SIMULATIONS WITH DISCRETE AND CONTINUOUS MODELS

A master equation for the discrete number of channels in each of the four states can be formulated from the gating scheme in Fig. 1(b). These equations are simulated by using random Markovian transitions for all N channels in a cluster and time-advancing Eqs. (2) and (3). Figure 2(a) shows that this approach produces Ca^{2+} dynamics resembling experimentally observed Ca^{2+} puff sequences. Parameters for the gating dynamics we have used: $a_5 = 100$ (μM s)$^{-1}$, $k_a^- = b_5 = 20$ s^{-1}, $k_i^+ = 0.1$ (μM s)$^{-1}$, $k_i^- = 1.7$ s^{-1}, and $c_{\rm s} = 300$ μM. These values have been taken to fit the single channel patch-clamp data and have been adjusted for the reduction from a subunit to a channel-based Markov chain and the fitting of recent puff data in SH-SY5Y cells [9,23].

To obtain an equivalent Langevin model, we wish to replace n in Eq. (2) by the product of the total number of channels N and the fraction of channels in the open state a. Replacing the discrete number of channels by its continuous counterpart Na entails that $c_{\rm d}$ can be larger than c_0 even if less than one channel is open. This misrepresentation is a source of inadequate continuous modeling (see below), and we therefore introduce a function that possesses a step at the crucial transition from zero to one open channel,

$$c_{\rm d}(a) = c_0 + c_1 Na\tfrac{1}{2}\{1 + \tanh[(Na - 1)/\epsilon)]\} \tag{4}$$

[see Fig. 2(b)]. Introducing a step calcium dependence on an open-channel number serves to make the Langevin model consistent with integer values present in the master equation [14] and is similar to the rounding to integer numbers that was used in stochastic Hodgkin-Huxley models [24,25] to improve accuracy in simulations. The tanh function is used to avoid a sharp step, that would lead to a discontinuity and possibly

numerical instability in a differential equation approach. The parameter ϵ in (4) is chosen at 0.1 in all of the following and characterizes the discreteness of the 0 to 1 step. In principle, the interface could be made sharper by reducing ϵ, but this needs smaller time steps for the differential equation approach and reduces efficiency in simulations. We have tested that a smaller ϵ value of 0.01 does not substantially change the outcome of the numerical simulations.

Rate equations with Langevin noise for each gating state can be derived from the reaction scheme in the standard way. For the fraction of channels in the respective states one obtains

$$\frac{da}{dt} = k_{\rm a}^{+} cz - k_{\rm a}^{-} a + k_{\rm i}^{-} g - k_{\rm i}^{+} c_{\rm s} a + G_{\rm za} + G_{\rm ag}, \quad (5)$$

$$\frac{dz}{dt} = -k_{a}^{+} cz + k_{a}^{-} a + k_{i}^{-} z - k_{i}^{+} cz - G_{\rm za} + G_{\rm hz}, \quad (6)$$

$$\frac{dh}{dt} = k_{i}^{+} cz - k_{i}^{-} h + k_{a}^{-} g - k_{a}^{+} ch + G_{\rm gh} - G_{\rm hz}, \quad (7)$$

where $g = 1 - a - h - z$ because of conservation of probability. The $G_{..}$ terms are Langevin noises representing stochasticity of the channel opening and closing. Following the approach of Fox and Lu [26] one obtains terms for Gaussian white noise with zero means and with

$$\langle G_{\rm za}(t) G_{\rm za}(t') \rangle = (k_{\rm a}^{+} cz + k_{\rm a}^{-} a)\delta(t - t')/N, \quad (8)$$

$$\langle G_{\rm ag}(t) G_{\rm ag}(t') \rangle = (k_{\rm i}^{+} c_{\rm s} a + k_{\rm i}^{-} g)\delta(t - t')/N, \quad (9)$$

$$\langle G_{\rm hz}(t) G_{\rm hz}(t') \rangle = (k_{\rm i}^{+} cz + k_{\rm i}^{-} h)\delta(t - t')/N, \quad (10)$$

$$\langle G_{\rm gh}(t) G_{\rm gh}(t') \rangle = (k_{\rm a}^{+} ch + k_{\rm a}^{-} g)\delta(t - t')/N. \quad (11)$$

These equations are simulated together with Eqs. (3) and (4) using the Euler-Maruyama method with a time step of 10^{-5} s. Special care has to be given to the treatment of variables that leave the [0,1] interval because of a fluctuation. Here we avoided unphysical channel fractions by repeating time steps whenever any of the gating variables leaves the unit interval. This method has been used before in numerical simulations of neuronal channel dynamics [26]. To test the approach, we have determined the number of level crossings in sample simulations (data not shown). On average, less than 3% of the time steps have to be repeated because of boundary crossings. We found no noticeable increase in the number of crossings during specific segments of the trajectory.

Figure 2(c) shows a typical time evolution in the Langevin simulations for comparison with the Markovian simulation. It should be noted that with a standard representation $n = Na$, or $c_{\rm d}(a) = c_0 + c_1 Na$, a state of intermediate level and noisy activity results (d), which does not reflect the original dynamics. Thus an adequate representation of the original dynamics is only obtained by invoking the $[Ca^{2+}]$ step at the transition from zero to one open channel [14].

The puff frequencies for both methods are calculated from simulation runs of 1000 s and are shown in Fig. 3. A single puff event is defined to begin whenever the open-channel number

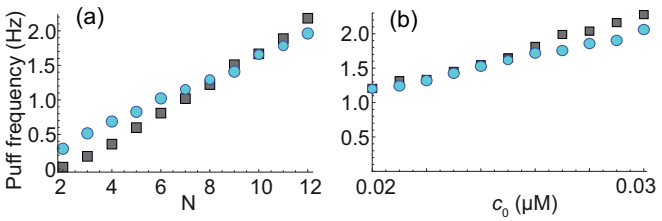

FIG. 3. (Color online) (a) Frequencies of puffs depending on the number of channels in a cluster N. Puffs are defined as openings of more than one channel (□: Langevin; ○: discrete). (b) Discrete and continuous simulations agree well for a wide range of parameters. For example, frequency of puffs increases with rest level concentration c_0 ($N = 10$ channels) and for both simulation methods.

n or Na exceeds 1.5 and to end when it falls below 0.5 for more than 5 ms. The obtained frequencies agree very well with experimental data in [22]. The Langevin model works best for channel numbers around $N = 8$. For larger $N > 12$, the definition of puffs from the time series becomes difficult because of a transition in dynamical behavior (see below). We have further tested the validity of our approach for a wide range of system parameters. For example, in variation of rest level concentration c_0 in a range around 0.025 μM both methods show an increase in puff frequency [Fig. 3(b)].

Equations (3)–(7) can be analyzed in the deterministic limit where all noise terms $G_{..}$ are set to zero. Figure 4 shows the evolution of components a, g, and h starting in an initial state where most of the channels reside in the rest state z but a sufficiently large fraction of channels resides in the open state a. The evolution exhibits the fast activation of the open state fraction followed by a slower g component and an even slower h component. This time course can be considered the deterministic backbone of elementary Ca^{2+} release.

To further analyze the dynamical system without noise, we have eliminated the c dynamics by a quasistationary approximation, where $c = c_0 + c_1 Na \frac{1}{2}\{1 + \tanh[(Na - 1)/\epsilon]\}$. We have further reduced the gating equations to a three-state model (z,a,h'), where state h' encompasses the two inhibitory states g and h. Rates from the compound state h' to a and z are

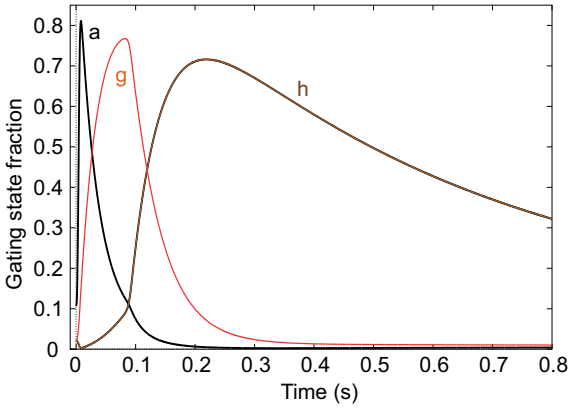

FIG. 4. (Color online) The dynamical evolution of gating state fractions a, g, and h after initialization $a = 0.11$, $g = 0.02$, $h = 0.02$, and $z = 0.85$.

given by $k_1 = k_i^- g_0$ and $k_2 = k_i^-(1 - g_0)$, respectively, where $g_0 = k_a^+ c/(k_a^+ c + k_a^-)$ is the fraction of g occupancy relative to h. Rates from a and z towards h' are the original rates towards g and h, respectively. The resulting system consists of two ordinary differential equations (ODEs),

$$\frac{da}{dt} = k_a^+ cz - k_a^- a + k_1 h' - k_i^+ c_s a, \tag{12}$$

$$\frac{dh'}{dt} = k_i^+ cz - k_1 h' - k_2 h' + k_i^+ c_s a, \tag{13}$$

with $z = 1 - a - h'$. The two-dimensional system can be studied using standard bifurcation theory. Figure 5 shows the nullclines (a green, h' red) as well as an exemplary trajectory with initial conditions $a = 0.12$ and $h' = 0.1$. The left and right green segments join at $h' \approx -29$ so that the activator nullcline forms an inverted N. The nullclines intersect at a stable fixed point very close to the origin. Because of the stability of the fixed point, a sufficiently large perturbation is needed to initiate a Ca^{2+} puff by jumping beyond the middle segment of the activator nullcline. Thus, the shapes of the nullclines and of the trajectory resemble those known from excitable systems where perturbations or noise drive the nonlinear dynamics [27].

It is often found that excitable systems can be tuned to regimes of oscillatory or bistable dynamics by an alteration of the nullclines. If, in Fig. 4(b), the inhibitor nullcline shifts or turns to the right or the activator nullcline moves to the left, their nullclines may intersect three times creating a second stable fixed point on the right branch of the a nullcline. In the two-dimensional ODEs (12) and (13), this happens by decreasing c_s, decreasing c_1, or increasing the number of channels N (see the inset in Fig. 5). The number N can be interpreted as the number of activatable channels in the cluster, which can be increased experimentally by larger IP_3 concentration. This raises the intriguing possibility that upon IP_3 increase the system undergoes a transition from excitable to bistable behavior. In the latter case, one finds that an initial perturbation away from the low-inhibition fixed point ($h' \approx 0.1$) results in a large initial spike along the a nullcline and back to the second fixed point with small open fraction a and large inhibition ($h' \approx 0.9$).

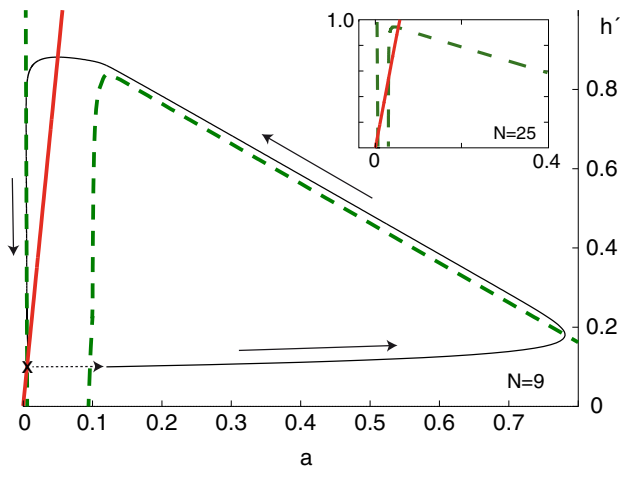

FIG. 5. (Color online) Nullclines and exemplary trajectory of a Ca^{2+} puff for the three-state model. The green dashed and red solid curves are nullclines of a and h' variables, respectively. The crossing point of the two nullclines is a fixed point marked by an "x." A perturbation away from the fixed point (marked by the dotted arrow) triggers an excitable trajectory (thin black line with arrows). In the final segment the trajectory follows the a nullcline towards the fixed point.

We propose that the bistable behavior embodies Ca^{2+} release in the form of global waves observed in many nonexcitable cells and in ryanodine receptor mediated release. According to current understanding, Ca^{2+} signals propagate by diffusion of Ca^{2+} from active clusters to inactive adjacent clusters, but it is unclear how to accommodate the very different time courses and periods of puffs and waves in this framework [7,10]. In this respect it is interesting to note that release through IP_3R channels in *Xenopus* oocytes involves two different processes. For small $[IP_3]$, calcium currents last only shortly (around 100 ms) whereas for larger $[IP_3]$, i.e., during a wave, Ca^{2+} efflux is initially as large as during a puff but proceeds as a leak flux for several seconds [15]. This transition has been attributed to the effects of coupling, but a detailed mathematical model of the puff-to-wave transition shows the two phases have not been devised. Our finding of a bifurcation to bistability for increased channel number, however, suggests a different mechanism consistent with the two distinct release phases. Here the transition is caused by a change in local behavior of the single cluster. Furthermore, it is conceivable that the persistent leak flux causes much larger Ca^{2+} release than during a puff and that the larger coupling is thus the consequence and not the cause of the puff-to-wave transition. This issue will be discussed in detail in a future paper.

IV. CONCLUSIONS

To summarize, we have devised a differential equation model for subcellular Ca^{2+} release that explicitly takes into account the very small number of channels in a cluster. We uncover what is perhaps the smallest system in the living world for which molecular interactions can be cast into an equation system with deterministic excitability. This approach also clarifies the role of noise in the system and provides the missing link that clearly demonstrates the noise-induced nature of Ca^{2+} puffs.

We emphasize that, because of the nonstandard representation of the $[Ca^{2+}]$ versus open-channel-number relation, the setup of our model and the resulting dynamics are very different from prior attempts at Langevin modeling of Ca^{2+} puffs [12,13]. These studies exploited the Li-Rinzel scheme, which was derived to model Ca^{2+} oscillations on much longer time scales [28]. Additionally, the activator variable was dynamically enslaved to the Ca^{2+} concentration, whereas noise was incorporated in the inhibitor variable. In our model, the dominant noise effect is caused by the activator fluctuations. Most importantly, however, our model is by construction adapted to the small channel numbers typically found in IP_3R clusters, whereas the earlier models described the stochastic behavior in the master equations for large channel numbers only. This difference is particularly evident from the fact that

our model in the deterministic limit decisively depends on the number of channels N, which is not usually the case for such continuous approximations.

Our approach of using continuous gating variables can be likened to that in studies of neuronal dynamics with schemes as for example that from Hodgkin and Huxley. Accordingly, our approach of two-dimensional phase-plane analysis follows that of the FitzHugh-Nagumo model [29]. A phase-plane analysis was also carried out for a cluster of ryanodine receptor channels [30,31]. However, there the structure of intersecting nullclines and the existence of bistability in the two-dimensional phase plane was not observed. Our incorporation of multiple $[Ca^{2+}]$ scales into differential equations may hence spur the development of realistic and transparent models for subcellular, intracellular, and intercellular dynamics of Ca^{2+}.

ACKNOWLEDGMENTS

Support from the Deutsche Forschungsgemeinschaft (Grants No. IRTG 1740 and No. RU1660) is gratefully acknowledged.

[1] M. Berridge, M. Bootman, H. Roderick *et al.*, Nat. Rev. Mol. Cell Biol. **4**, 517 (2003).
[2] I. Parker, I. Ivorra *et al.*, Science **250**, 977 (1990).
[3] H. Cheng, W. Lederer, and M. Cannel, Science **262**, 740 (1993).
[4] M. Bär, M. Falcke, H. Levine, and L. S. Tsimring, Phys. Rev. Lett. **84**, 5664 (2000).
[5] M. Falcke, Biophys. J. **84**, 42 (2003).
[6] M. Nivala, C. Y. Ko, M. Nivala, J. N. Weiss, and Z. Qu, Biophys. J. **102**, 2433 (2012).
[7] S. Rüdiger, Phys. Rep. **534**, 39 (2014).
[8] S. Rüdiger, J. W. Shuai, and I. M. Sokolov, Phys. Rev. Lett. **105**, 048103 (2010).
[9] G. Ullah, I. Parker, D. Mak, and J. Pearson, Cell Calcium **52**, 152 (2012).
[10] P. Cao, G. Donovan, M. Falcke, and J. Sneyd, Biophys. J. **105**, 1133 (2013).
[11] R. Hinch and S. J. Chapman, Eur. J. Appl. Math. **16**, 427 (2005).
[12] J. W. Shuai and P. Jung, Phys. Rev. Lett. **88**, 068102 (2002).
[13] L. Meinhold and L. Schimansky-Geier, Phys. Rev. E **66**, 050901 (2002).
[14] R. Thul and M. Falcke, Phys. Rev. E **73**, 061923 (2006).
[15] S. Dargan and I. Parker, J. Physiol. **553**, 775 (2003).
[16] G. De Young and J. Keizer, Proc. Natl. Acad. Sci. USA **89**, 9895 (1992).
[17] J. Foskett, C. White, K. Cheung, and D. Mak, Physiol. Rev. **87**, 593 (2007).
[18] S. Rüdiger, P. Jung, and J. Shuai, PLoS Comput. Biol. **8**, e1002485 (2012).
[19] S. Rüdiger, Ch. Nagaiah, G. Warnecke, and J. W. Shuai, Biophys. J. **99**, 3 (2010).
[20] I. Smith and I. Parker, Proc. Natl Acad. Sci. USA **106**, 6404 (2009).
[21] V. Nguyen, R. Mathias, and G. Smith, Bull. Math. Biol. **67**, 393 (2005).
[22] A. L. Hodgkin and A. F. Huxley, J. Physiol. **117**, 500 (1952).
[23] G. D. Dickinson, D. Swaminathan, and I. Parker, Biophy. J. **102**, 1826 (2012).
[24] I. C. Bruce, Ann. Biomed. Eng. **35**, 315 (2007).
[25] Y. Huang, S. Rüdiger, and J. Shuai, Phys. Lett. A **377**, 3223 (2013).
[26] R. F. Fox and Y.-n. Lu, Phys. Rev. E **49**, 3421 (1994).
[27] B. Lindner, J. Garcia-Ojalvo, A. Neimann, and L. Schimansky-Geier, Phys. Rep. **392**, 321 (2004).
[28] Y.-X. Li and J. Rinzel, J. Theor. Biol. **166**, 461 (1994).
[29] J. Keener and J. Sneyd, *Mathematical Physiology: Cellular Physiology* (Springer, New York, 2008).
[30] R. Hinch, Biophys. J. **86**, 1293 (2004).
[31] M. D. Stern, E. Ríos, and V. A. Maltsev, J. Gen. Physiol. **142**, 257 (2013).